To show the usefulness of the system in viscoelastic measurement, accurately-controlled tensile tests on stress fibers obtained from smooth muscle cells are presented at constant strain rates, strains, or loading.

2. Materials and methods

2.1. Tensile test system

A home-built tensile test system (Fig. 1a) was mounted on an inverted microscope (IX-71, Olympus, Japan) fixed on a vibration-isolated table (h-TDI-1510LA, Herz, Japan) in a dark room. Tensile

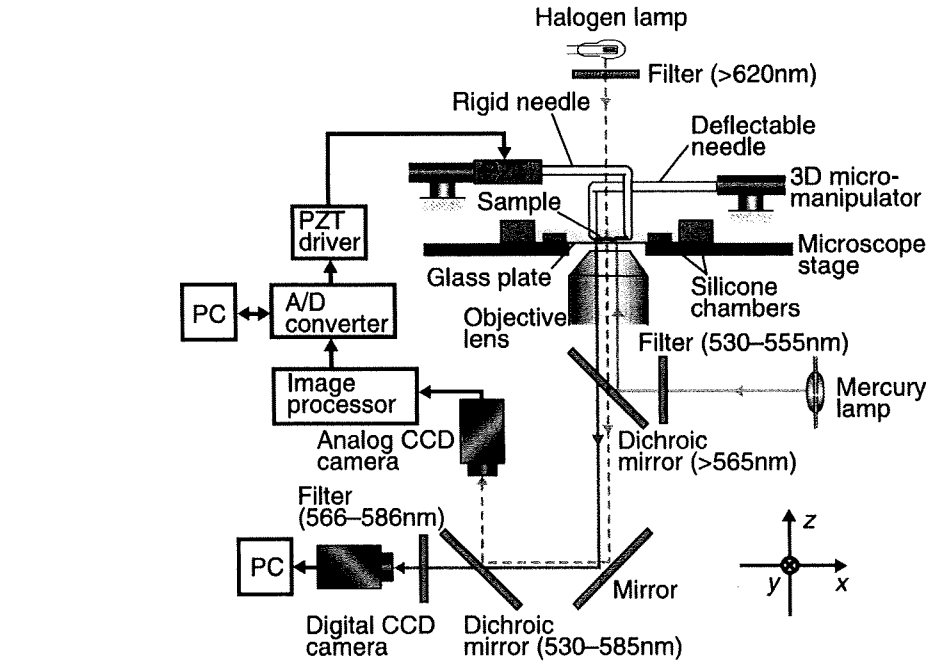

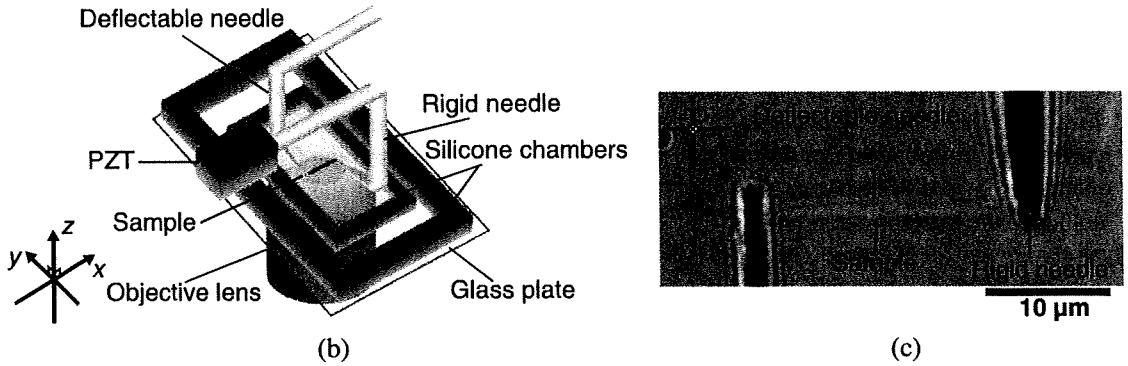

Fig. 1. The micro-mechanical tester. (a) Schematic of the overall experimental setup. (b) The upside of the microscope stage showing a sample stress fiber held between two micro-needles. Not depicted in precise relative scale. (c) A bright-field image of the actual single stress fiber captured by the needles.

tests of single stress fibers are conducted using two glass micro-needles moved by 3D hydraulic micro-manipulators (MWO-3, Narishige, Japan). The needles with a diameter of 1–3 μm at the tip are made from glass rods (1 mm in diameter) using a glass-electrode puller (P-97, Sutter Instrument, CA, USA). One of the needles has a long axial length and is therefore flexible, with a spring constant of 3–6 nN/μm, i.e., of the order of the elastic stiffness of typical stress fibers [8]. This deflectable needle is thus used as a force sensor. The other needle has a short axial length and hence is rigid with a spring constant of at least two orders of magnitude higher than that of the deflectable needle. Its position is accurately controlled using a piezoelectric ceramic actuator (PZT, AE0505D44H40, NEC Tokin, Japan; the maximum achievable movement speed = 50 μm/ms). The needles are observed through a 60× water immersion objective lens under halogen light illumination and taken by an analog CCD camera (TM1650, Toshiba, Japan) at a sampling rate of 60 Hz. The distance between the positions of the needle tips, corresponding to the axial length of a sample stress fiber, is measured by an image processor (C3161, Hamamatsu, Japan) from the images captured in real time. The precision in the measurement of the needle displacement was 0.026 μm with a dynamic range of ~50 μm. The sample stress fiber, which is fluorescently labeled prior to measurement, is observed with mercury lamp illumination. The epifluorescence images of the sample, taken by a digital CCD camera (C4742-95-12NR, Hamamatsu, Japan) through inserted dichroic mirrors, are synchronized offline with the other images taken for the needle position control in order to determine how the labeled constituents of interest are involved in the displacement and force. The needle position control for viscoelastic measurements is processed by a PID (proportional-integral-derivative) controller under LabVIEW software (version 8.6, Professional Development System, National Instruments, Japan), and a correction command is sent to the PZT via an analog-to-digital/digital-to-analog converter board (PCIe-6251, National Instruments, Japan).

2.2. *Preparation of actin stress fibers*

Bovine aortic smooth muscle cells were cultured in Dulbecco's modified Eagle medium supplemented with 10% fetal bovine serum and 1% each of penicillin and streptomycin. The cells were originally seeded onto a rectangular glass plate of 170 μm in thickness, which was immersed in a culture dish of 60 mm in diameter. The cells were used at passage 4–10 for experiments. Sample stress fibers were prepared according to Katoh et al. [27] with modification. Briefly, the cells were first rinsed with a HEPES buffer (25 mM HEPES, 125 mM potassium acetate, 12 mM glucose, 1 mM manganese chloride and 2.5 mM magnesium chloride; pH = 7.0) [17]. The cells were then treated at 4°C with a low-ionic strength solution (2.5 mM triethanolamine, 1 μg/ml leupeptin, 1 μg/ml pepstatin and 1 mM DTT; pH = 8.2) for 5 min and subsequently treated for 2 min with a cytoskeleton-stabilizing buffer (50 mM potassium chloride, 10 mM imidazole, 1 mM EGTA, 1 mM magnesium chloride, 20 mM PIPES, 1 μg/ml leupeptin, 1 μg/ml pepstatin and 10 mM DTT; pH = 6.5) [40] containing 0.1% Triton X-100. With these treatments, stress fibers were extracted and exposed to solutions, as the other cytoplasmic constituents including the nucleus are removed. The extracted stress fibers were then washed with the cytoskeleton-stabilizing buffer without Triton X-100 but with either 1 nM Alexa Fluor 546-conjugated phalloidin (A22283, Molecular Probes, OR, USA) or 20 nM amino functionalized PEG-coated quantum dots 585 (Qdot, Q21511MP, Invitrogen, USA) that was conjugated with phalloidin following a manufacturer's protocol to visualize actin filaments in stress fibers. In separate experiments, we confirmed that the stress fibers obtained following the above procedure are capable of contracting in response to Mg-ATP, as previously reported by Katoh et al. [27], thus keeping intactness in terms of the actomyosin contractility. The glass plate having the extracted stress fibers in the rigor state on the surface was then enclosed with a

home-built rubber fence that could adhere to the glass surface to make a confined space of 12×24 mm^2 in inner area and of 1 mm in height (Fig. 1b). A total of 300 μm^3 cytoskeleton-stabilizing buffer with oxygen-removal reagents (2.3 mg/ml glucose, 0.018 mg/ml catalase and 0.1 mg/ml glucose oxidase) [30,31] was added as a working solution into the space. Another rubber fence, larger in size having an inner area of 25×35 mm^2 and a height of 5 mm, was also mounted to enclose the small chamber. The smaller one containing the working solution and samples was then covered with mineral oil (Fig. 1a and b). The glass/rubber-made chamber was fixed on the microscope stage.

2.3. *Viscoelastic tests*

Before the experiments, the tips of the glass needles were coated with platinum-palladium using an ion coater (E-1030, Hitachi, Japan). This coating increases optical contrast, facilitating the optical measurement of their positions and displacements. The needles are then treated with glutaraldehyde-aminosilane by which protein components of stress fibers are covalently and nonspecifically bound to the needle surface through imine groups [17]. The needles were then washed with deionized water and bent into a double L-shape by heating them with a lighter. One of the extracted stress fibers in the chamber was carefully lifted up from the bottom using the coated glass needle, and thus a stress fiber isolated from the cell was held between the two needles (Fig. 1c). Here, the captured one was confirmed to be a single filament by checking its fluorescence image.

Prior to beginning a measurement, a slight stretching was given to the captured stress fiber beyond its slack length by moving the rigid needle. The stretching was confirmed by a resulting slight deflection of the deflectable needle. We released the stretching by returning the rigid needle carefully toward the original position. The initial length of the sample stress fiber was then determined as the distance between the inner edges of the needles.

Here, three types of viscoelastic tests on the stress fibers in the rigor state were performed at room temperature (20°C) to demonstrate the performance of the system: (i) strain rate-controlled tensile tests (Fig. 2), (ii) stress relaxation tests (Fig. 3) and (iii) creep tests (Fig. 4). Under the strain rate-controlled condition, the sample stress fiber was stretched in its axial direction by moving the rigid needle at a constant strain rate of 1%/s or 10%/s (Fig. 2a). During the stretching, the axial tension in the stress fiber produced by the stretching was measured based on the deflection of the deflectable needle and recorded on the computer. A constant strain rate was realized by measuring the sample length at a given time based on captured images, dividing it by the initial length to obtain the strain at that time, calculating the difference between the strain and a desired one for accomplishing a constant increase in strain over time, and driving the PZT to reduce the difference to zero (Fig. 2b). Likewise, the vision-based feedback control was used for the relaxation and creep tests. In the relaxation test, in which the way tension in stress fibers relaxed over time was studied, an initial stretching strain of 20% or 40% was first given to a sample stress fiber within 1 s (Fig. 3a). The strain was then kept constant by the visual feedback control, while measuring possible changes in tension in the stress fiber (Fig. 3b). Conversely, in the creep test, the mode of elongation occurring under a constant loading was studied. An initial tensile loading of 10 or 15 nN was first applied to a sample stress fiber within 1 s (Fig. 4a), and then the time course of change in strain was tracked under constant force realized by the feedback control (Fig. 4b). The experimental parameters used here (i.e., 10%/s strain rate, ~20% strain and ~10 nN tension) were chosen based on the typical behavior of stress fibers [8].

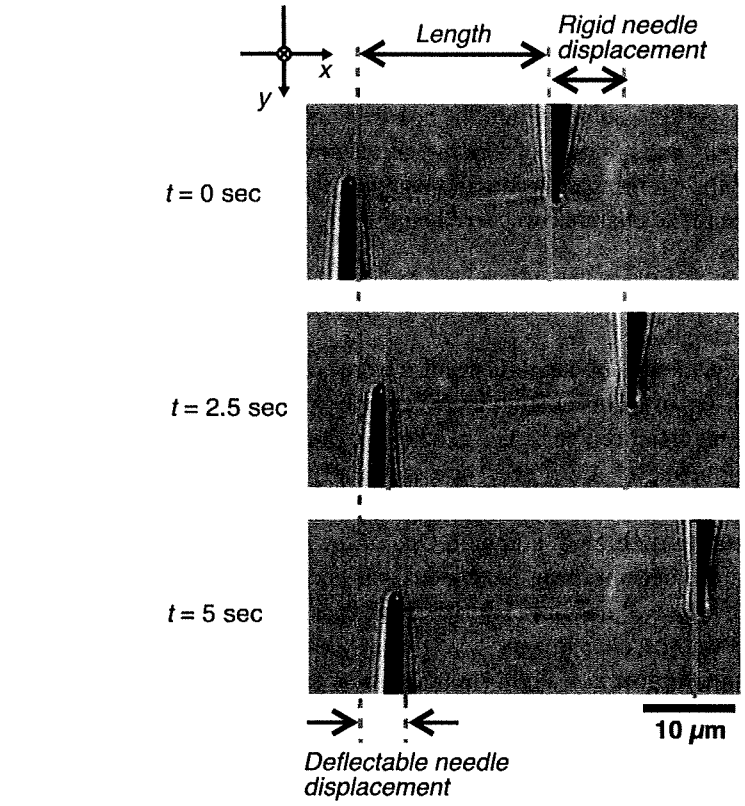

Fig. 2. Strain rate-controlled test. (a) A sequence of bright-field images of a single stress fiber under a stretching at a constant strain rate. Note that the sample length, corresponding to the distance between the blue and green solid lines, was elongated at a constant rate; meanwhile, the force detected by the deflectable needle displacement (i.e., the distance between the blue broken line and solid line) was not increased at a constant rate. (b) Block diagram for the strain rate control.

3. Results

To realize the versatile viscoelastic measurements, the base section of the rigid needle to which the PZT is connected must be automatically and suitably controlled with a feedback system while measuring the sample displacement and loading. The use of the vision-based system enables us to execute the measurements with a high dynamic range. In the strain rate-controlled test, a sample stress fiber was captured between the two needles and stretched up to 50% strain at a constant strain rate of 1%/s (Fig. 5a) or 10%/s (Fig. 5b) realized by the control. As expected, these typical examples of the test demonstrated that the sample strain followed a desired linear increase over time along which the strain rate was kept

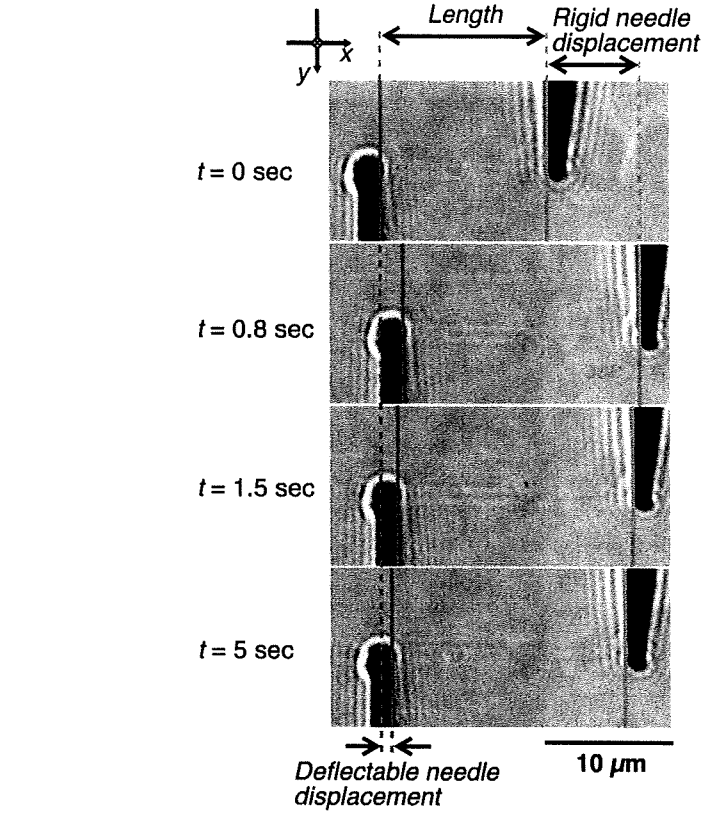

Fig. 3. Relaxation test. (a) A sequence of bright-field images of a single stress fiber under a relaxation test. A single stress fiber was stretched from t = 0–0.8 s, and the strain was kept unchanged thereafter as shown by a constant distance between the blue and green solid lines. (b) Block diagram for the strain control or relaxation test.

unchanged. In contrast, the force or tension in the stress fiber did not in general show a linear curve, indicating that the stress fibers tested here are a nonlinear material whose stiffness is dependent on strain magnitude. It has been reported that the stress fibers of smooth muscle cells have a lateral width of ~400 nm (e.g., [7]). The width is so small that it is difficult to accurately evaluate the changes in the cross-sectional area during the tests and hence to normalize the force by the cross-sectional area.

In the stress relaxation test, the base part of the rigid needle was first displaced outward to give an initial stretching strain of 20% (Fig. 6a) or 40% (Fig. 6b), giving rise to a tension in the stress fiber. The needle base was then automatically controlled to keep the constant strain, and the subsequent tension–time history or relaxation curve was recorded. These typical examples of the test demonstrated that the

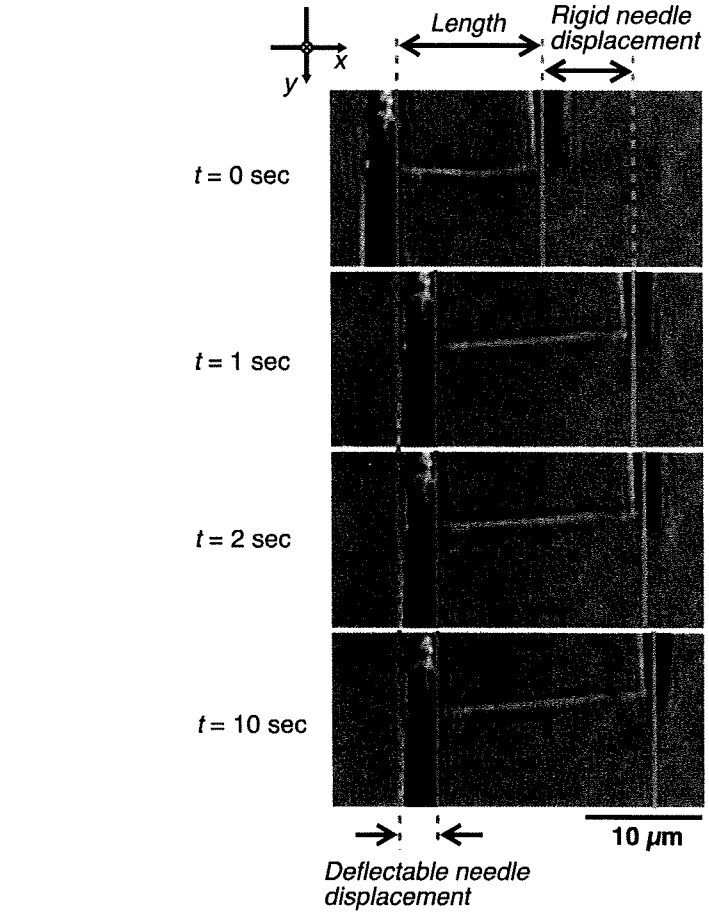

(a)

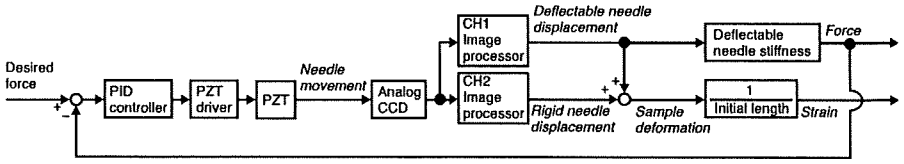

(b)

Fig. 4. Creep test. (a) A sequence of bright-field images of a single stress fiber under a creep test. A single stress fiber was stretched from $t = 0$–1 s, and the force was kept unchanged thereafter as confirmed by the unchanged position of the deflectable needle (as shown by a blue solid line). (b) Block diagram for the force control or creep test.

strain was kept at the desired value without any noticeable overshoots and deviations. Meanwhile, the tension was elevated just after the application of the strain, and then it gradually fell with time to finally reach a plateau. The initial tension thus relaxed with time, a typical feature of viscoelastic materials.

In the creep test, the rigid needle base was quickly displaced outward to give an initial loading of 10 (Fig. 7a) or 15 nN (Fig. 7b), again yielding a tension in the stress fiber. The needle base was controlled thereafter to keep the initial magnitude of the tension. Meanwhile, possible changes in the strain were

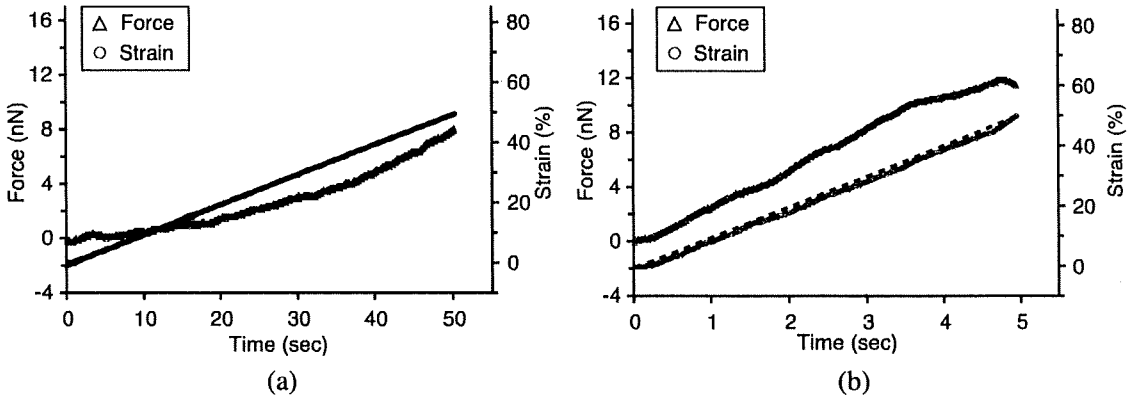

Fig. 5. Force–strain curves at constant strain rates of 1%/s (a) and 10%/s (b). The dashed lines represent the respective desired strain paths with the same slope as the set strain rate.

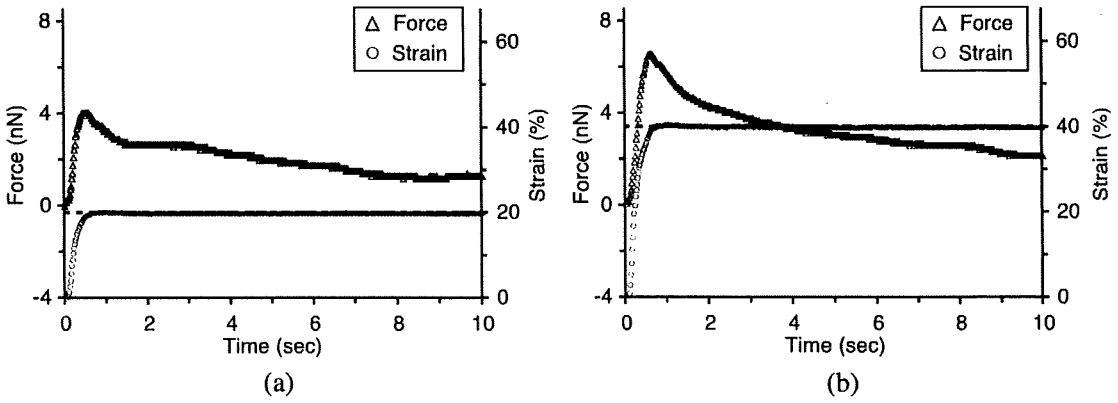

Fig. 6. Relaxation curves under constant stretching strains of 20% (a) and 40% (b). The dashed lines represent the respective controlled strain values.

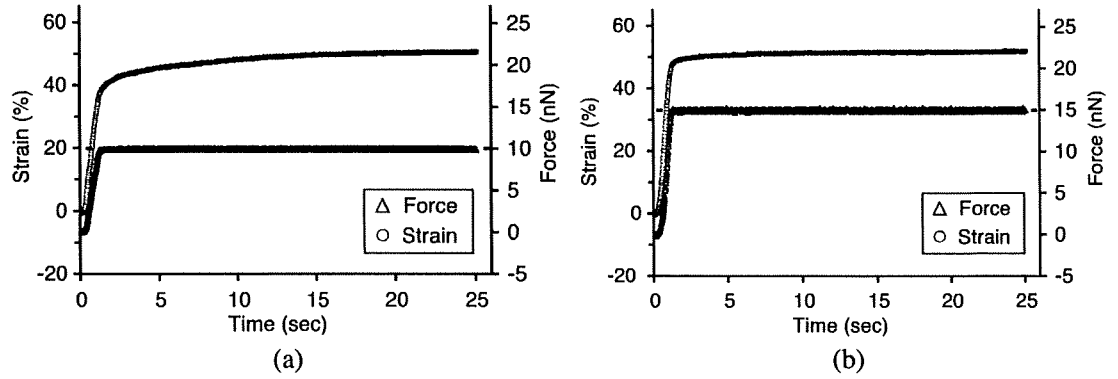

Fig. 7. Creep curves under constant tensions of 10 (a) and 15 nN (b). The dashed lines represent the respective controlled force values.

recorded over time, providing a strain–time history or creep curve of the sample. The typical examples of the test demonstrated that the tension was successfully kept at the set value during the measurement. The tensed stress fiber was gradually elongated as time passed even under a tension of the same magnitude. The elongation finally reached a plateau, thus exhibiting viscoelastic creep behavior. To demonstrate the feasibility of simultaneous measurements of those viscoelastic properties and local structural changes along the sample stress fibers that could be detected by fluorescence imaging, relaxation tests were performed together with acquisition of Qdot movements (Fig. 8). Actin filaments in the stress fibers were sparsely labeled with the Qdots, which are a nano-crystal of semiconductor with bright fluorescence and high photo-stability and hence can be used as a fluorescent marker for long-term tracking of biomolecules [17]. Qdots bound to stress fibers were illuminated with the mercury light through an excitation filter (of 530–555 nm wavelength range) and a dichroic mirror (that reflects light of <565 nm) and imaged with the digital CCD camera through another dichroic mirror (that passes 530–585 nm light) and an emission filter (of 566–586 nm range) (Fig. 1a). At the same time, the needles were illuminated with the halogen light through a filter (that passes >620 nm light) and imaged with the analog CCD camera through the same dichroic mirrors. The dual imaging provided movements of the sparsely-distributed Qdots (Fig. 8a), which could be used as a marker for strain analysis, with the corresponding relaxation curve (Fig. 8b). The result showed that, with an initial stretch to apply a 30% strain, the spacing between Qdots was enlarged as the stress fiber was elongated. The change in the spacing was not uniform in magnitude along the axial direction, suggesting that the stiffness varies place by place, just as other studies using AFM and live cell imaging have reported [9]. The distances between the Qdots remained almost unchanged even in the tension relaxation process. However, it is noteworthy that a distinct local displacement perpendicular to the stretch direction was observed in the relaxation process (arrowheads, Fig. 8b), potentially due to a structural twist caused by a deformation in the axial direction [27].

4. Discussion

The novel mechanical tester developed in the present study was equipped with (i) a pair of micro-needles to manipulate a filamentous sample in a project plane, (ii) a visual feedback control system to keep user-defined length or force histories and (iii) dichroic mirrors and image detectors to capture changes in the sample structure during measurement. The manipulation within the horizontal plane permits absolute positioning of the needle probe, which is vital to accurate quantification of mechanical features including viscoelastic properties. Conventional AFM, one of the major techniques for mechanical tests, manipulates a sample within the vertical plane, and hence it is often difficult to tell the absolute position of the cantilever probe subject to thermal drift.

Furthermore, the test within the project plane has a potential application to observation of structural changes or physiological events responsible for the mechanical behavior. Recently, a dual piezo-driven cantilever system has been used to examine mechanical features, such as deformability and stiffness, characteristic of meiotic spindles in Xenopus egg extracts together with fluorescence microscopy on microtubules using a mercury lamp [21]. As far as we know, however, no fluorescence microscopy under a force/displacement-controlled condition has been reported. In order to demonstrate the usefulness of our setup aimed at such sophisticated tests, a Qdot-labeled stress fiber was observed over the course of the relaxation experiment (Fig. 8). This control was made possible through a vision-based feedback system in which the position of the micro-needles as force/displacement sensors was detected optically with transmitted light, whereas changes in the sample structure were determined by means of dichroic mirrors and a separate image detector in the epifluorescence microscopic mode. By adjusting the stiffness of

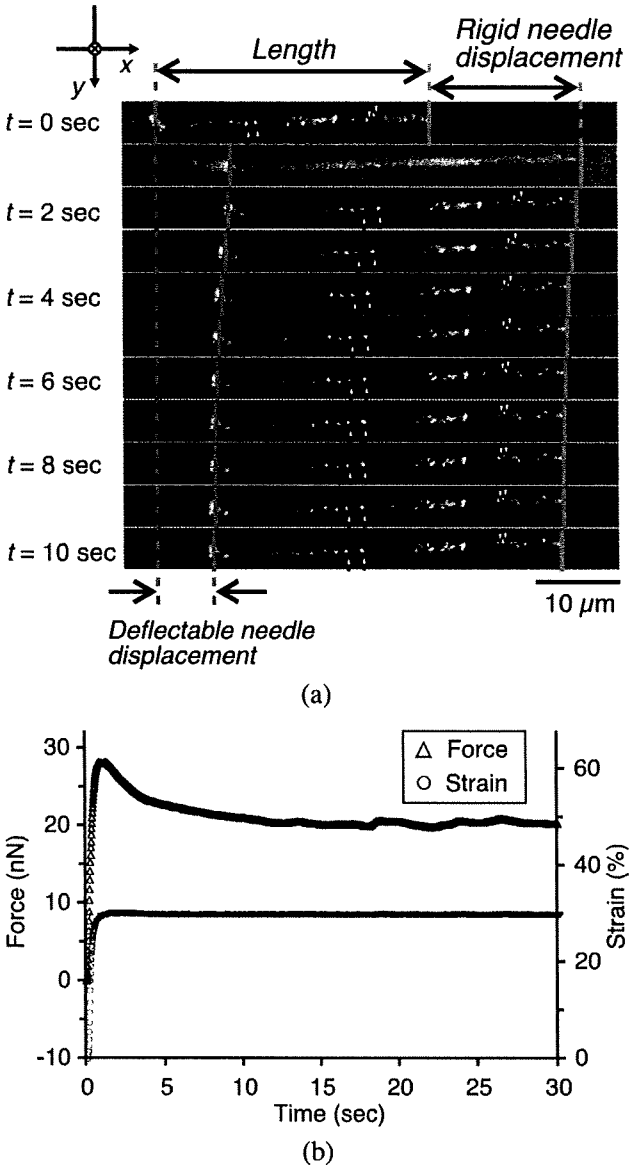

Fig. 8. Relaxation test with fluorescence imaging. (a) Sequential images of a Qdot-labeled stress fiber under relaxation test. The stress fiber was stretched from t = 0–1 s to give a 30% strain, and the strain was kept constant afterwards. The blue and green dashed lines represent the original positions of the needles. The blue and green solid lines represent the inner edges of the respective needles. Note that some parts in the stress fiber deformed to the same extent and direction as the overall unidirectional stretch (as shown by arrows); meanwhile, another part (shown by arrowheads) just showed little deformation in the stretching process (t = 0–2 s), yet a considerable displacement perpendicular to the stretch direction was seen in the subsequent relaxation process (t = 2–10 s). (b) The corresponding force relaxation curve. The dashed line represents the controlled strain value (i.e., 30%).

the deflectable needle accordingly, forces can be measured over a wide range of magnitude. All the advances presented here should allow us to implement detailed measurements on mechanical properties of

stress fibers as well as other important biomaterials, thus making our setup a versatile micro-mechanical tester.

Alcaraz et al. [1] pointed out that fluid viscous force might affect the deflection of a classical AFM cantilever, which in turn could contribute to the measured force. It is estimated from their analyses and measurements that a force of at most 0.1 nN order of magnitude may be applied to an AFM triangular cantilever having a projected length of 200 μm and moving at 0.1–100 Hz with an amplitude of 50 nm. Since the spring constant of the needle used in the present study is 3–6 nN/μm, a 0.1 nN force would induce a deflection of 0.017–0.033 μm, which is of the same order with our measurement precision (i.e., 0.026 μm). However, a possible viscous force in our system using the thin needle should be undoubtedly smaller in magnitude than that appears in the AFM experiment using such a relatively larger cantilever. Thus, we concluded that the fluid viscous force is practically neglected in the present study. Actually, we could not detect any delays in movement between the tip and base of the deflectable needle that is free of load and hence is subject only to a possible fluid viscous force. It is however noteworthy that the fluid force could become to affect the data when we apply the current system to measurements on single protein filaments (e.g., [30,31]) in which a small force of pico-Newton order of magnitude appears instead of nano-Newton force as in the current actin stress fiber mechanics.

There have been more and more studies indicating that mechanical forces play critical roles in cellular physiology and pathogenesis [16,18,38,46]. The forces are transmitted via subcellular structural components such as stress fibers, which in turn activate mechano-sensing sites. As cells usually exhibit profound viscoelastic behavior [14,25,50], those forces should be distributed within the cytoplasm in a strain rate-dependent manner and relaxed to some extent over time. To estimate the strain rate-dependency as well as the time required for the force transmission within cells, knowledge of the viscoelastic properties of the force-bearing components is necessary [12,15,32,33]. Contributions of stress fibers, in particular, to the viscoelastic force transmission are thought to be of importance as they run between separate focal adhesion sites that are physically connected to the extracellular matrix and hence are subject to extracellular forces. As the viscoelastic properties of stress fibers themselves remain poorly understood, the versatile mechanical tester developed here is useful and can be applied to carry out thorough measurements on them, except that a heated plate for the microscope stage should be added to the current system to check the dependence on temperature. Structural changes responsible for the macroscopic mechanical behavior, as indicated in the present fluorescence microscopy (Fig. 8), will be also another important subject of future investigation. In addition to the passive role of stress fibers as a force-transmitter, the Mg-ATP-induced actomyosin contraction in the interior of the stress fiber structure also remains to be examined quantitatively [9,27]. Our setup with the capability of realizing isometric contractions of isolated stress fibers (equivalent to the relaxation test in terms of technique) would be able to help address the active role of the stress fibers as well.

5. Conclusions

A tensile test system was developed that incorporated a pair of micro-needles to manipulate a sample in a project plane. The micro-needle was moved to follow user-defined forces or displacements using a visual feedback control. Visoelastic measurements of isolated stress fibers in the rigor state were conducted under constant strain rates, strains, or forces. Fluorescence imaging was also carried out together with viscoelastic measurements by the use of dichroic mirrors and multiple image detectors, demonstrating the usefulness of the system as a powerful tool to examine the quantitative relationship between

mechanical behavior and related structural changes. Further thorough measurements using this versatile system on stress fibers and other important biomaterials will be the subject of future investigations.

Acknowledgements

The authors thank Kazushi Ito for stimulating discussion. This study was supported by a Grant-in-Aid for Scientific Research (Specially Promoted Research, #20001007) and Tohoku University Global COE Program "Global Nano-Biomedical Engineering Education and Research Network Centre".

References

[1] J. Alcaraz, L. Buscemi, M. Grabulosa, X. Trepat, B. Fabry, R. Farre and D. Navajas, Microrheology of human lung epithelial cells measured by atomic force microscopy, *Biophys. J.* **84** (2003), 2071–2079.
[2] A. Ashkin, J.M. Dziedzic, J.E. Bjorkholm and S. Chu, Observation of a single-beam gradient force optical trap for dielectric particles, *Opt. Lett.* **11** (1986), 288–290.
[3] N. Caille, O. Thoumine, Y. Tardy and J.J. Meister, Contribution of the nucleus to the mechanical properties of endothelial cells, *J. Biomech.* **35** (2002), 177–187.
[4] E. Canetta, A. Duperray, A. Leyrat and C. Verdier, Measuring cell viscoelastic properties using a force-spectrometer: influence of protein-cytoplasm interactions, *Biorheology* **42** (2005), 321–333.
[5] C.R. Carlisle, C. Coulais, M. Namboothiry, D.L. Carroll et al., The mechanical properties of individual, electrospun fibrinogen fibers, *Biomaterials* **30** (2009), 1205–1213.
[6] E.P. Debold, J.B. Patlak and D.M. Warshaw, Slip sliding away: load-dependence of velocity generated by skeletal muscle myosin molecules in the laser trap, *Biophys. J.* **89** (2005), L34–L36.
[7] S. Deguchi, T. Ohashi and M. Sato, Newly designed tensile test system for *in vitro* measurement of mechanical properties of cytoskeletal filaments, *JSME Int. J. Ser. C* **48** (2005), 396–402.
[8] S. Deguchi, T. Ohashi and M. Sato, Tensile properties of single stress fibers isolated from cultured vascular smooth muscle cells, *J. Biomech.* **39** (2006), 2603–2610.
[9] S. Deguchi and M. Sato, Biomechanical properties of actin stress fibers of non-motile cells, *Biorheology* **46** (2009), 93–105.
[10] N. Desprat, A. Richert, J. Simeon and A. Asnacios, Creep function of a single living cell, *Biophys. J.* **88** (2005), 2224–2233.
[11] P. Fernandez, P.A. Pullarkat and A. Ott, A master relation defines the nonlinear viscoelasticity of single fibroblasts, *Biophys. J.* **90** (2006), 3796–3805.
[12] R. Fodil, V. Laurent, E. Planus and D. Isabey, Characterization of cytoskeleton mechanical properties and 3D-actin structure in twisted adherent epithelial cells, *Biorheology* **40** (2003), 241–245.
[13] J.M. Goffin, P. Pittet, G. Csucs, J.W. Lussi et al., Focal adhesion size controls tension-dependent recruitment of alpha-smooth muscle actin to stress fibers, *J. Cell Biol.* **172** (2006), 259–268.
[14] F. Guilak, J.R. Tedrow and R. Burgkart, Viscoelastic properties of the cell nucleus, *Biochem. Biophys. Res. Commun.* **269** (2000), 781–786.
[15] H. Haga, S. Sasaki, K. Kawabata, E. Ito et al., Elasticity mapping of living fibroblasts by AFM and immunofluorescence observation of cytoskeleton, *Ultramicroscopy* **82** (2000), 253–258.
[16] K. Hayakawa, H. Tatsumi and M. Sokabe, Actin stress fibers transmit and focus force to activate mechanosensitive channels, *J. Cell Sci.* **121** (2008), 496–503.
[17] H. Hirata, H. Tatsumi and M. Sokabe, Dynamics of actin filaments during tension-dependent formation of actin bundles, *Biochim. Biophys. Acta* **1770** (2007), 1115–1127.
[18] S. Hu, J. Chen, B. Fabry, Y. Numaguchi et al., Intracellular tomography reveals stress focusing and structural anisotropy in cytoskeleton of living cells, *Am. J. Physiol. Cell Physiol.* **285** (2003), C1082–C1090.
[19] J.D. Humphrey, Vascular adaptation and mechanical homeostasis at tissue, cellular, and sub-cellular levels, *Cell Biochem. Biophys.* **50** (2008), 53–78.
[20] A. Ishijima, T. Doi, K. Sakurada and T. Yanagida, Sub-piconewton force fluctuations of actomyosin *in vitro*, *Nature* **352** (1991), 301–306.
[21] A. Ishijima, H. Kojima, T. Funatsu, M. Tokunaga et al., Simultaneous observation of individual ATPase and mechanical events by a single myosin molecule during interaction with actin, *Cell* **92** (1998), 161–171.

[22] T. Itabashi, J. Takagi, Y. Shimamoto, H. Onoe et al., Probing the mechanical architecture of the vertebrate meiotic spindle, *Nat. Methods* **6** (2009), 167–172.
[23] S. Kamimura, Direct measurement of nanometric displacement under an optical microscope, *Appl. Optics* **26** (1987), 3425–3427.
[24] S. Kamimura and K. Takahashi, Direct measurement of the force of microtubule sliding in flagella, *Nature* **293** (1981), 566–568.
[25] H. Karcher, J. Lammerding, H. Huang, R.T. Lee, R.D. Kamm and M.R. Kaazempur-Mofrad, A three-dimensional viscoelastic model for cell deformation with experimental verification, *Biophys. J.* **85** (2003), 3336–3349.
[26] K.E. Kasza, A.C. Rowat, J. Liu, T.E. Angelini et al., The cell as a material, *Curr. Opin. Cell Biol.* **19** (2006), 1–7.
[27] K. Katoh, Y. Kano, M. Masuda, H. Onishi and K. Fujiwara, Isolation and contraction of the stress fiber, *Mol. Biol. Cell* **9** (1998), 1919–1938.
[28] R. Kaunas and H.J. Hsu, A kinematic model of stretch-induced stress fiber turnover and reorientation, *J. Theor. Biol.* **257** (2009), 320–330.
[29] R. Kaunas, P. Nguyen, S. Usami and S. Chien, Cooperative effects of Rho and mechanical stretch on stress fiber organization, *Proc. Natl. Acad. Sci. USA* **102** (2005), 15895–15900.
[30] A. Kishino and T. Yanagida, Force measurements by micromanipulation of a single actin filament by glass needles, *Nature* **334** (1988), 74–76.
[31] H. Kojima, A. Ishijima and T. Yanagida, Direct measurement of stiffness of single actin filaments with and without tropomyosin by *in vitro* nanomanipulation, *Proc. Natl. Acad. Sci. USA* **91** (1994), 12962–12966.
[32] V.M. Laurent, E. Planus, R. Fodil and D. Isabey, Mechanical assessment by magnetocytometry of the cytosolic and cortical cytoskeletal compartments in adherent epithelial cells, *Biorheology* **40** (2003), 235–240.
[33] G. Lenormand and J.J. Fredberg, Deformability, dynamics, and remodeling of cytoskeleton of the adherent living cell, *Biorheology* **43** (2006), 1–30.
[34] X. Liu and G.H. Pollack, Mechanics of F-actin characterized with microfabricated cantilevers, *Biophys. J.* **83** (2002), 2705–2715.
[35] N.L. McKnight and J.A. Frangos, Strain rate mechanotransduction in aligned human vascular smooth muscle cells, *Ann. Biomed. Eng.* **31** (2003), 239–249.
[36] J.P. Mills, L. Qie, M. Dao, C.T. Lim and S. Suresh, Nonlinear elastic and viscoelastic deformation of the human red blood cell with optical tweezers, *Mol. Cell. Biomech.* **1** (2004), 169–180.
[37] H. Miyazaki, Y. Hasegawa and K. Hayashi, A newly designed tensile tester for cells and its application to fibroblasts, *J. Biomech.* **33** (2000), 97–104.
[38] S. Na, O. Collin, F. Chowdhury, B. Tay, M. Ouyang, Y. Wang and N. Wang, Rapid signal transduction in living cells is a unique feature of mechanotransduction, *Proc. Natl. Acad. Sci. USA* **105** (2008), 6626–6631.
[39] K. Nagayama, S. Yanagihara and T. Matsumoto, A novel micro tensile tester with feed-back control for viscoelastic analysis of single isolated smooth muscle cells, *Med. Eng. Phys.* **29** (2007), 620–628.
[40] J. Pourati, A. Maniotis, D. Spiegel, J.L. Schaffer et al., Is cytoskeletal tension a major determinant of cell deformability in adherent endothelial cells?, *Am. J. Physiol. Cell Physiol.* **274** (1998), C1283–C1289.
[41] N. Sakamoto, T. Ohashi and M. Sato, Effect of fluid shear stress on migration of vascular smooth muscle cells in cocultured model, *Ann. Biomed. Eng.* **34** (2006), 408–415.
[42] M. Sato and T. Ohashi, Biorheological views of endothelial cell responses to mechanical stimuli, *Biorheology* **42** (2005), 421–441.
[43] M. Sato and N. Ohshima, Flow-induced changes in shape and cytoskeletal structure of vascular endothelial cells, *Biorheology* **31** (1994), 143–153.
[44] M. Sato, N. Ohshima and R.M. Nerem, Viscoelastic properties of cultured porcine aortic endothelial cells exposed to shear stress, *J. Biomech.* **29** (1996), 461–467.
[45] M. Sato, K. Nagayama, N. Kataoka, M. Sasaki and K. Hane, Local mechanical properties measured by atomic force microscopy for cultured bovine endothelial cells exposed to shear stress, *J. Biomech.* **33** (2000), 127–135.
[46] Y. Sawada, M. Tamada, B.J. Dubin-Thaler, O. Cherniavskaya et al., Force sensing by mechanical extension of the Src family kinase substrate p130Cas, *Cell* **127** (2006), 1015–1026.
[47] G.H. Shue and F.V. Brozovich, The frequency response of smooth muscle stiffness during Ca^{2+}-activated contraction, *Biophys. J.* **71** (1999), 2361–2369.
[48] O. Thoumine and A. Ott, Time scale dependent viscoelastic and contractile regimes in fibroblasts probed by microplate manipulation, *J. Cell Sci.* **110** (1997), 2109–2116.
[49] M. Tokunaga, T. Aoki, M. Hiroshima, K. Kitamura and T. Yanagida, Subpiconewton intermolecular force microscopy, *Biochem. Biophys. Res. Commun.* **231** (1997), 566–569.
[50] Y. Tseng, J.S. Lee, T.P. Kole, I. Jiang and D. Wirtz, Micro-organization and viscoelasticity of the interphase nucleus revealed by particle nanotracking, *J. Cell Sci.* **117** (2004), 2159–2167.

[51] S. Yang and M.T.A. Saif, Microfabricated force sensors and their applications in the study of cell mechanical response, *Exp. Mech.* **49** (2009), 135–151.
[52] S. Yasuda, S. Sugiura, N. Kobayakawa, H. Fujita et al., A novel method to study contraction characteristics of a single cardiac myocyte using carbon fibers, *Am. J. Physiol. Heart. Circ. Physiol.* **281** (2001), H1442–H1446.

Experimental Mechanics (2009) 49:125–134
DOI 10.1007/s11340-008-9143-3

Morphological Responses of Vascular Endothelial Cells Induced by Local Stretch Transmitted Through Intercellular Junctions

Y. Ueki · N. Sakamoto · T. Ohashi · M. Sato

Received: 6 June 2007 / Accepted: 24 March 2008 / Published online: 23 April 2008

Abstract It has been well established that mechanical stimuli including fluid shear stress and cyclic stretch play a key role in endothelial cell (EC) remodeling. However, in contrast to global remodeling to these mechanical stimuli, little is known of how local mechanical forces are transmitted through cells to induce cell remodeling leading to alteration in cell functions. In this study, we demonstrated that EC remodeling can be exerted by local tension generated in a neighboring EC. In this technique, a glass microneedle was used to apply local stretch in an EC in confluent monolayer and the resulting tension is transmitted to a neighboring EC across intercellular junctions. Local stretch induced reorientation and elongation of ECs parallel to the direction of stretch associated with reorganization of stress fibers. In addition, recruitment of Src homology 2-containing tyrosine phosphatase-2, binding to intercellular adhesion molecules platelet-endothelial cellular adhesion molecules-1, was selectively observed at the force-transmitted intercellular junctions after application of local stretch. These findings suggest that intercellular junctions can not only transmit but also sense local forces, and are potentially involved in EC mechanotransduction pathways.

Keywords Endothelial cell remodeling · Stress fibers · Mechanotransduction · Intercellular junction · Adhesion molecules

Y. Ueki (✉) · N. Sakamoto · T. Ohashi · M. Sato
Department of Bioengineering and Robotics,
Graduate School of Engineering, Tohoku University,
6-6-01 Aramaki-aoba,
Sendai 980-8579, Japan
e-mail: ueki@bml.mech.tohoku.ac.jp

N. Sakamoto
e-mail: naoya@bml.mech.tohoku.ac.jp

T. Ohashi
e-mail: ohashi@bml.mech.tohoku.ac.jp

M. Sato
Department of Biomedical Engineering,
Graduate School of Biomedical Engineering, Tohoku University,
6-6-01 Aramaki-aoba,
Sendai 980-8579, Japan
e-mail: sato@bml.mech.tohoku.ac.jp

Introduction

Endothelial cells (ECs) lining inner surfaces of blood vessels are exposed to a variety of mechanical stimuli including fluid shear stress due to blood flow, cyclic stretch due to the wall deformation, and hydrostatic pressure due to blood pressure. Since the relationship between EC morphology and mechanical conditions has been implicated in vascular pathology such as atherosclerosis, in vitro model systems have been widely used to investigate the effects of mechanical stimuli on EC remodeling. Most previous studies have exclusively applied global mechanical stimuli including fluid shear stress [1–4], cyclic stretch [5, 6] and hydrostatic pressure [7, 8] to cultured EC monolayer. For example, under exposure to fluid shear stress, ECs exhibit elongation and alignment parallel to the direction of flow concomitant with reorganization of actin stress fibers (SFs) [2, 4]. It is also well known that ECs exposed to cyclic stretch elongate and align perpendicular to the direction of stretch [5]. Furthermore, pressure-imposed ECs elongate with random orientation [7]. Thus, ECs respond very specifically to the type of mechanical stimuli, raising the question of how externally applied mechanical forces transmit in cells and where the transmitted forces are sensed and converted into biochemical signals. It has been suggested that mechanotransduction of ECs may occur at

specific sites located in cell membrane (e.g. stretch activated channels (SACs)), attachment points of ECs to extracellular matrix (e.g. integrins), intercellular junctions (e.g. platelet-endothelial cellular adhesion molecules-1, PECAM-1) and more likely a combination of these sites. However, the details of these mechanotransducers in cell signaling pathways remain unclear, because, in part, there is a possibility that these mechanotransducers can be simultaneously activated by the globally applied mechanical stimuli. Therefore, it is necessary to develop an experimental method, with which each mechanotransducer can be selectively stimulated.

Intercellular junctions of ECs involve adherens-junctions, tight-junctions, gap-junctions and PECAM-1 junctions. Particularly, adherens-junctions composed of VE-cadherin which is connected to actin-cytoskeleton via α/β catenins are thought to exclusively mediate forces at intercellular junctions by forming homophilic binding, probably because mechanical coupling by adherens-junctions may be stiffer than the other junctions. Recently, there has been a growing attention on the role of intercellular adhesion molecules with implications of EC mechanotransduction signalling pathways. PECAM-1 is known to form homophilic binding between neighboring ECs [9] in the vicinity of adherens-junctions and be connected to actin-cytoskeletons via β/γ catenins [10]. Previous reports revealed that ECs under sparse conditions do not show morphological changes in response to fluid shear stress [11, 12]. Osawa et al. [13] reported that PECAM-1 is rapidly tyrosine-phosphorylated when ECs are exposed to fluid shear stress or hyper osmotic shock, and bind to a protein tyrosine phosphatase Src homology 2-containing tyrosine phosphatase-2 (SHP-2) to activate intracellular signal cascades. Tzima et al. [14] reported that PECAM-1-mediated mechanotransduction is involved in the upstream of the integrin signaling cascade, leading to cytoskeletal reorganization in flow conditioned ECs. This leads to an idea that transmitted forces at adherens-junctions may stimulate PECAM-1 phosphorylation, leading to SHP-2 activation followed by morphological changes of ECs. Thus, PECAM-1 may be responsible for morphological responses to mechanical stimuli transmitted through intercellular junctions serving as one of principal mechanotransducers.

To test this hypothesis, in this study, local stretch was applied to an EC by using a microneedle to selectively stimulate intercellular junctions between the EC and a neighboring EC. After application of mechanical stimuli, morphological changes of the neighboring EC were fluorescently observed to test the hypothesis that local stimuli are transmitted via intercellular junctions and induce EC remodeling. In addition, localization of SHP-2 was observed to assess whether PECAM-1 is involved in the mechanotransduction pathways.

Materials and Methods

Cell Culture and Transfection

Human umbilical vein endothelial cells (HUVECs) were obtained from umbilical veins with trypsin treatment adapted from Sakamoto et al. [15]. Cells were cultured in Medium 199 (Invitrogen, USA) containing 20% fetal bovine serum (Sigma-Aldrich, USA), 10 ng/ml basic fibroblast growth factor (Austral Biologicals, USA) and penicillin–streptomycin (Invitrogen), and were used from the third to the sixth passage. For experiments, cells were plated on a glass base culture dish (ø=35 mm, Asahi Techno Glass, Japan) coated with 0.1% gelatin (Sigma-Aldrich). A plasmid encoding enhanced green fluorescent protein (EGFP)-actin (Clontech, USA) was transfected into HUVECs with a liposomal method using Lipofectin (Invitrogen) according to the manufacturer's protocol for visualization of actin cytoskeleton.

Local Stretch Experiment

Figure 1 shows the experimental setup used to apply local stretch. A glass microneedle with a diameter of ca. 1 μm

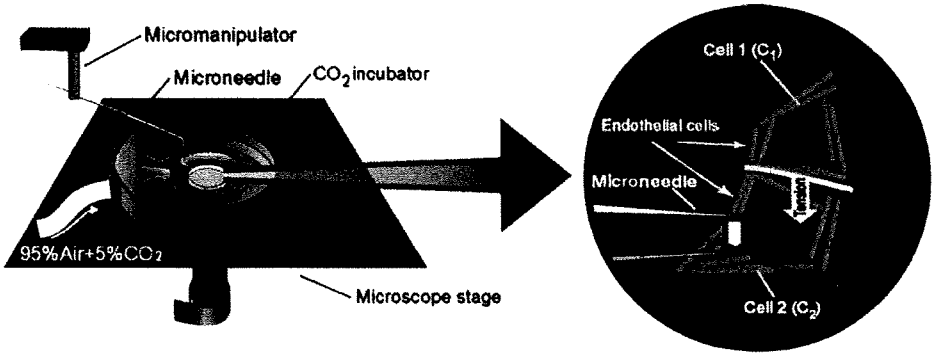

Fig. 1 Schematic illustrations of experimental system for local stretch application. A microneedle was used to apply local stretch to C_2, possibly inducing remodeling of C_1 via intercellular junctions. The experiments were performed in a CO_2 incubator at 37°C and 5% CO_2

was made from a glass tube (ø=1 mm, GD-1, Narishige, Japan) using a pipette puller (PP-83, Narishige, Japan) and manipulated by a 3-D hydraulic micromanipulator. A pair of ECs (cell 1 (C_1) and cell 2 (C_2)) in the figure) expressing EGFP-actin were selected under a confocal laser scanning microscope (CLSM, FV1000, Olympus, Japan), and the nucleus of C_2 was then moved horizontally by 10 μm by manipulating the glass microneedle to locally stretch C_1. This procedure allows us to mimic cell deformation induced by externally applied local tension via intercellular junctions between C_1 and C_2. In a separate study, particle tracer velocimetry (PTV) method was performed to calculate distribution of intracellular deformation induced by local stretch by using a software (Flowvec, Library, Japan) (Fig. 2). The result showed that high displacement was observed specifically at the intercellular junctions between C_1 and C_2, confirming force transmission across the junctions. After application of local stretch, fluorescent images were obtained up to 60 min at intervals of 5 min with the CLSM to assess features of C_1 remodeling process. All procedures were performed in a CO_2 incubator (MI-IBC, Olympus) mounted on the microscope stage to maintain the cell culture environment at 37°C and 5% CO_2.

Image Analysis

Image analysis was performed to evaluate morphological and cytoskeletal changes of C_1 using the following parameters: angle of cell orientation, cell aspect ratio, angle of SF orientation and uniformity index of SF. Angle of cell orientation and cell aspect ratio were calculated with the public domain program Image J version 1.37v (National Institute of Health, USA). A cell outline was manually extracted from a fluorescence image of GFP-actin by tracing the cell edge. An equivalent ellipse for the cell outline was automatically determined with a function of the software. An angle between the major axis of the ellipse and the direction of stretch was then defined as the angle of cell orientation. A ratio of length of the minor axis to the major axis was defined as the cell aspect ratio, with being 1.0 for circles and approaching zero for highly elongated shape. Analyses were performed on the fluorescent images obtained at every 5 min after application of local stretch. See Appendix for details of the angle of SF orientation and the uniformity index of SF.

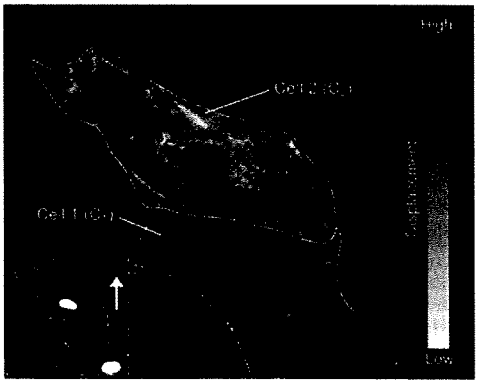

Fig. 2 Distribution of intracellular displacement calculated by using PTV method. Longer arrows represent higher displacement. Applied local stretch in C_2 was found to be transmitted to C_1 at intercellular junctions

SACs Blocking Experiment

In order to inhibit function of SACs, 20 μM $GdCl_3$ (Wako pure chemical, Japan) was added to cell culture medium at 30 min before application of local stretch.

Immunofluorescence

Localization of SHP-2 was examined with immunofluorescence. ECs were pre-incubated with 1 mM $NaVO_3$ (Wako Pure Chemical, Japan) for 30 min to enhance tyrosine phosphorylation before application of local stretch. Five minutes after the mechanical loading, ECs were then fixed in 4% paraformaldehyde (Wako Pure Chemical) containing 1 mM $NaVO_3$ for 15 min at 4°C. Next, ECs were permeabilized with 0.1% Triton X (Wako Pure Chemical), blocked with Block ace (Dainippon Sumitomo Pharma, Japan), and stained with anti-SHP-2 mouse monoclonal antibody (Santa Cruz Biotechnology, USA) and Alexa fluor 594 anti-mouse IgG (Invitrogen).

Statistical Analysis

Statistical comparisons in morphological parameters were performed using repeated measures analysis of variance (ANOVA) followed by Bonferroni's multiple comparison (0 min vs 30 min, 60 min). A p value less than 0.05 was considered as significant. Data are expressed a mean± SEM.

Results

Morphological Changes of ECs After Application of Local Stretch

Typical florescent images of EGFP-actin were shown in Fig. 3 at 0 min, 30 min and 60 min after application of local stretch. The observed cell C_1 initially elongated perpendicular to the direction of stretch [Fig. 3(a)] exhibited contraction at 30 min [Fig. 3(b)] followed by elongation

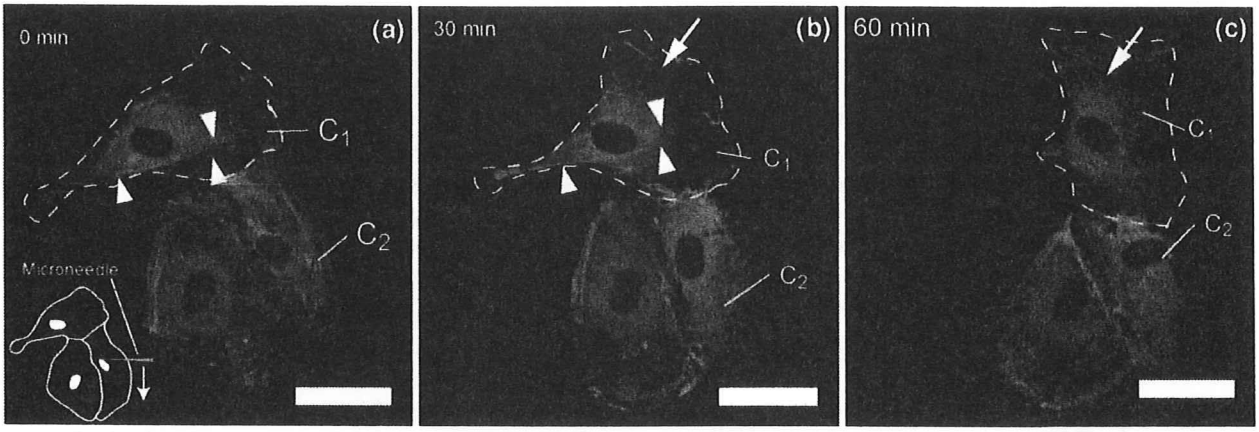

Fig. 3 Typical examples of fluorescent images of EGFP-actin at (**a**) 0 min, (**b**) 30 min, and (**c**) 60 min after application of local stretch. Broken lines indicate the edge of C_1. The horizontally elongated C_1 at 0 min (**a**) showed contraction at 30 min (**b**) and re-elongated parallel to the direction of the stretch at 60 min (**c**). Preexisting SFs at 0 min (**a**) disappeared at 30 min (**b**) and new SFs formation was observed at 60 min (**c**). Bar=40 μm

parallel to the direction of stretch at 60 min [Fig. 3(c)]. Concurrently with these morphological changes, SFs initially orientated perpendicular to the direction of stretch at 0 min [Fig. 3(a), arrowheads], and disappeared [Fig. 3(b), arrowheads] while formation of new SFs parallel to the direction of stretch was observed [Fig. 3(b), arrow] at 30 min. The new SF formation was continuously observed at 60 min [Fig. 3(c), arrow].

Figure 4 represents distribution of the angle of cell orientation and the cell aspect ratio of the observed cell C_1 at 0 min, 30 min and 60 min. From different types of initial cell morphology, the experimented data can be divided into two groups: Group A, ECs with angle of cell orientation >60° and aspect ratio <0.5; Group B, the rest of Group A. Roughly, distribution of the two groups is schematically drawn in the figure by ellipsoids. For both Groups, the angle of cell orientation significantly decreased from 0 min [Fig. 4(a), 71.3±4.4°, 53.3±4.6° for Groups A and B, respectively] to 60 min [Fig. 4(c), 52.1±6.8°, and 29.0±3.7° for Groups A and B respectively, $p<0.05$ vs 0 min for both groups]. For Group A, aspect ratio significantly increased from 0 min [Fig. 4(a), 0.42±0.02] to 30 min [Fig. 4(b), 0.57±0.07, $p<0.05$ vs 0 min] and then decreased at 60 min [Fig. 4(c), 0.53±0.08, NS vs 0 min]. On the other hand, for Group B, aspect ratio did not show a significant change from 0 min [Fig. 4(a), 0.57±0.05] to 30 min [Fig. 4(b), 0.55±0.07] and significantly decreased at 60 min [Fig. 4(c), 0.47±0.06, $p<0.05$ vs 0 min].

Time course of change in the SF parameters is summarized in Fig. 5. Angle of SF orientation for both groups significantly decreased at 60 min [Fig. 5(a), $p<0.05$, vs 0 min]. For Group A, change in the uniformity index was not significant between 0 min and 60 min [Fig. 5(b)] while the uniformity index significantly increased at 60 min for Group B [Fig. 5(b), $p<0.05$ vs 0 min].

SACs Blocking Experiment

SACs blocking experiment was performed on Group B with treatment of $GdCl_3$. Treated cells showed the similar time course of change in morphology, and morphological parameters showed no significant difference compared to those of non-treated control cells (data not shown). This result indicates that SACs should not be involved in the present remodeling.

Change in Distribution of SHP-2 After Application of Local Stretch

Figure 6 represents typical fluorescent images of EGFP-actin and anti-SHP-2 for control [Fig. 6(a,b,c)] and $GdCl_3$-treated ECs [Fig. 6(d,e,f)] after application of local stretch. For control ECs, recruitment of SHP-2 was clearly observed at the intercellular junctions between C_1 and C_2 [Fig. 6(b,c)]. For $GdCl_3$ -treated ECs, localization of SHP-2 was still observed at the intercellular junctions, suggesting that applied mechanical loading can be transduced into molecular signals [Fig. 6(e,f)].

Discussion

In this study, local tension transmitted via intercellular junctions was applied to ECs to induce morphological changes in a neighboring EC. The result showed that ECs elongate and orient parallel to the direction of stretch

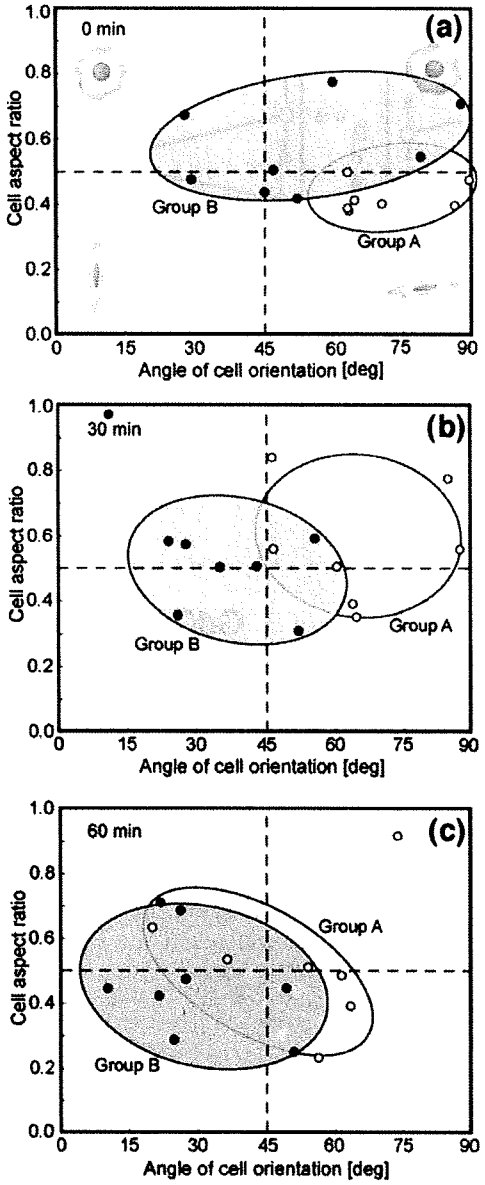

Fig. 4 Changes in morphological parameters of ECs at (a) 0 min, (b) 30 min and (c) 60 min after application of local stretch. Group A represents cells with angle of cell orientation >60° and aspect ratio <0.5 and Group B, the rest of Group A. The two groups showed different time course of changes in the morphological parameters

together with reorganization of stress fibers. Moreover, localization of SHP-2 was selectively observed at intercellular junctions, indicating that mechanotransduction might occur. Most previous studies relating to cell remodeling have utilized global mechanical stimuli including fluid shear stress [1–4] and cyclic stretch [5, 6]. With these conventional techniques, it is difficult to find both mechanotransmission pathways and mechanotransduction sites, probably because these events may occur by a combination of several candidate sensors. To overcome this difficulty, this study proposed a new experimental method to locally apply mechanical stimuli to ECs to identify the role of intercellular junctions involved in EC remodeling.

Interestingly, ECs finally aligned to the direction of stretch at 60 min after application of mechanical stimuli. The mechanism in the present EC remodeling process is unclear. It is well known that ECs exposed to cyclic stretch show alignment perpendicular to the direction of stretch [5]. Sokabe et al. [16] have suggested that when cells are subjected to cyclic stretch, actin cytoskeletons are disassembled during relaxation phase and disruption of actin fibers activates several downstream signals, leading to a cell shape change. On the other hand, ECs under continuous stretch have been shown to align parallel to the direction of stretch [17]. This is consistent with our results in which ECs align to the direction of local continuous stretch, strongly suggesting a critical role of relaxation phase in the EC alignment in response to the two different types of stretch. It is interesting to note that flow-imposed ECs are well known to show alignment to the direction of flow [1, 2, 4]. Although the types of mechanical loadings are different, this tendency is similar to the result of this study in terms of the directional alignment. Several numerical studies have well explained these phenomena of ECs in from the viewpoint of structural optimization. For example, Ohashi et al. [18] reported that ECs exposed to fluid shear stress change their morphology to reduce intracellular stress concentrations. Relating to biomolecular events, Tzima et al. [19] reported that, in ECs exposed to fluid shear stress, Rac1, which is small GTPase controls lamellipodia formation, is locally activated in the downstream region. Likewise, it is worth doing these numerical and extra experimental approaches to elucidate underlying mechanism in the present EC remodeling process. Further investigations may, therefore, include more detailed quantification of intracellular strain field and observations of local activity of Rho small GTPases including Rac1 responsible for reorganization for actin-cytoskeletons.

Time course of change in EC morphology was investigated to characterize EC remodeling process. The remodeling process depended on initial shapes of ECs and thus divided into the two groups: Group A and B. For Group A, ECs initially elongated perpendicular to the direction of stretch exhibited spontaneous contraction prior to elongation/alignment to the direction of stretch. In contrast, for Group B, ECs initially aligned to the direction of stretch immediately exhibited elongation parallel to the direction of stretch. It has been reported that ECs exposed to shear stress show the following time course of change: 1) contraction, 2) reorientation and 3) elongation [7]. Taken

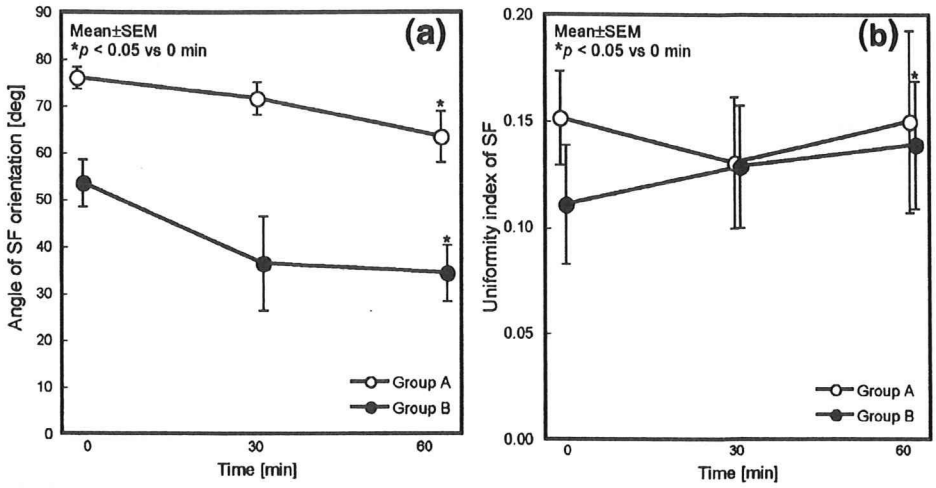

Fig. 5 Time course of changes in SF parameters. (**a**) Angle of SF orientation significantly decreased for both groups. (**b**) Change in uniformity index of SF was not significant for Group A, while the index significantly increased for Group B. See Appendix for details for determination of SF parameters. *$p<0.05$ vs 0 min

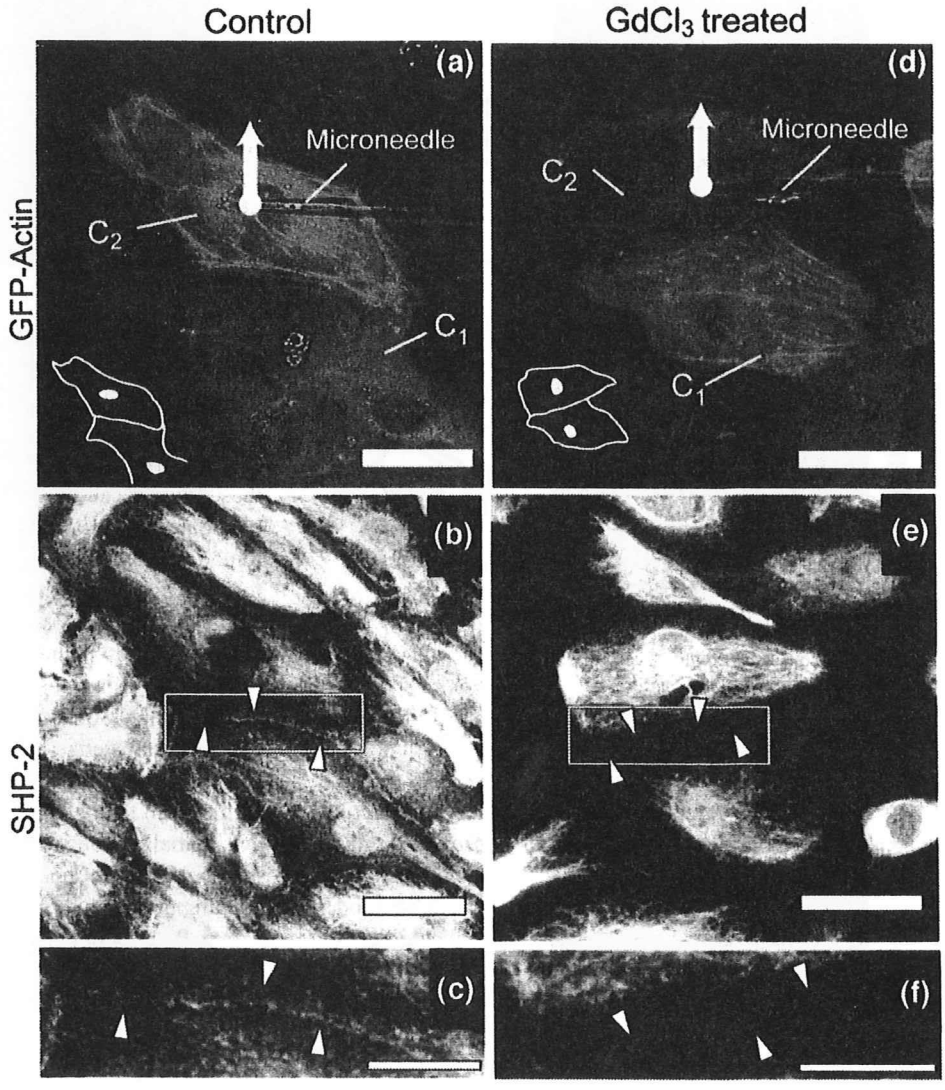

Fig. 6 Typical examples of fluorescent images of SHP-2 for control (**a**, **b**, **c**) and $GdCl_3$ treated ECs (**d**, **e**, **f**). Boxed regions in (**b**) and (**e**) are magnified in (**c**) and (**f**), respectively. Expression of SHP-2 was found to be localized at intercellular junctions (**b**, **d**; arrowheads). Bar=40 μm for (**a**, **b**, **d**, **e**), 20 μm for (**c**, **f**), respectively

these results and our results into consideration, there may exist specific time course of change depending on the type of externally applied mechanical stimuli. It is beyond our findings to see if the present remodeling process might be involved in the EC remodeling exposed to global mechanical stimuli including fluid shear stress. Figure 7 summarizes representative time course of EC remodeling process with GFP-actin together with schematic drawings representing cell morphology and actin organization. This result suggests that cell contraction or low angle of cell orientation should be prerequisite for EC elongation parallel to the direction of stretch. Noria et al. [20] suggested that flow-induced morphological changes of ECs were caused by reorganization of SFs. Moreover, Li et al. [21] reported that ECs transfected with dominant negative RhoA, responsible for SF formation, do not respond to fluid shear

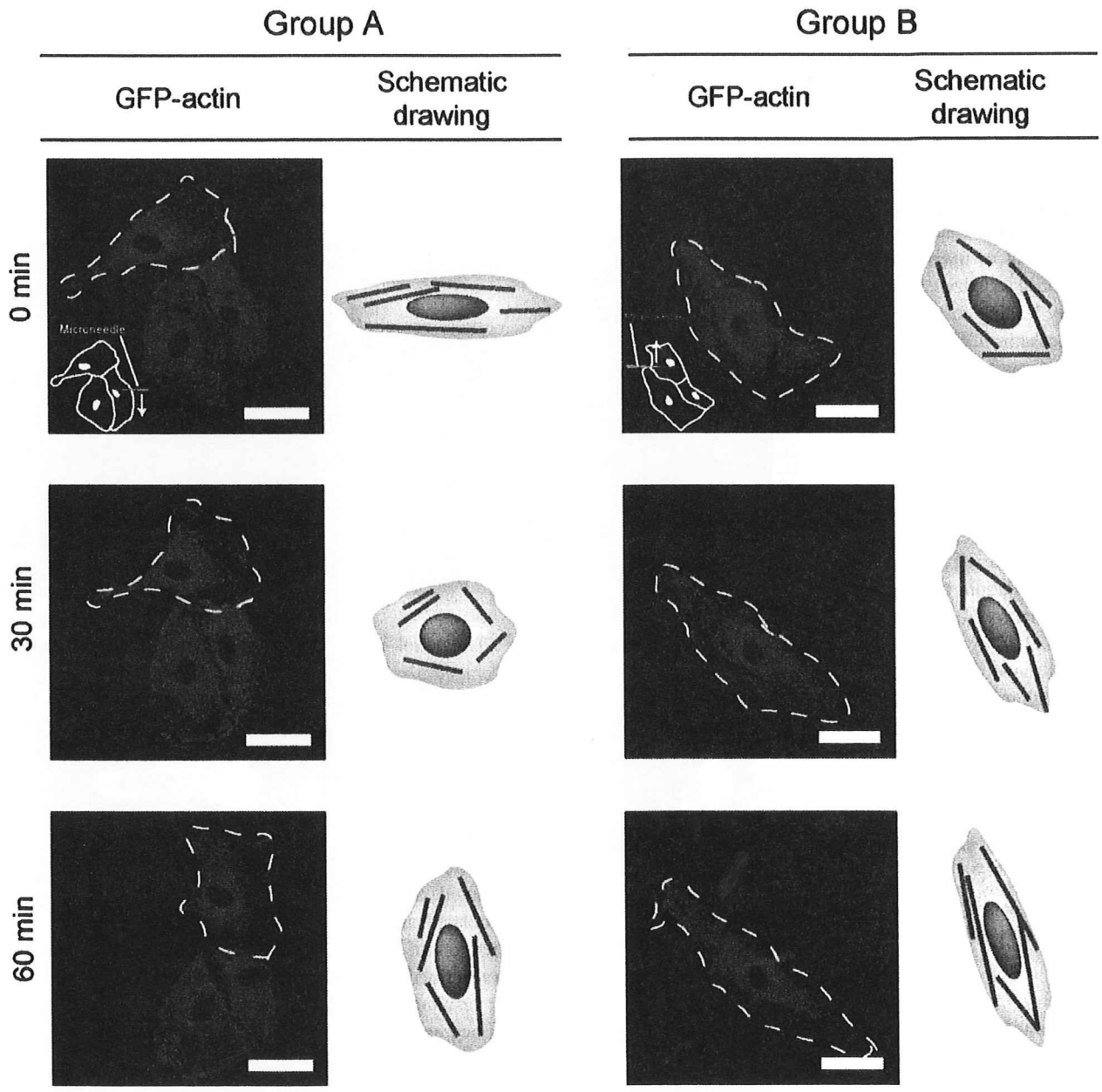

Fig. 7 Representative time course of EC remodeling process with fluorescent images and schematic drawings. Although time courses of change for the two groups are different, the observed ECs (C_1) finally elongated and orientated parallel to the direction of stretch